Radio- and photoluminescence properties of Ce/Tb co-doped glasses with huntite-like composition

Authors

Roberto Lorenzi[1,*], Nikita V. Golubev[2], Mariyam Z. Ziaytdinova[2], Vítězslav Jarý[3], Vladimir Babin[3], Georgii E. Malashkevich[4], Alberto Paleari[1,2], Vladimir N. Sigaev[2], Mauro Fasoli[1], Martin Nikl[3]

Affiliation
[1]*Department of Materials Science, University of Milano-Bicocca, via Cozzi 55, 20125 Milano, Italy*
[2]*P.D. Sarkisov International Laboratory of Glass-based Functional Materials, Mendeleev University of Chemical Technology of Russia, Miusskaya Square 9, 125047 Moscow, Russia*
[3]*Institute of Physics, Academy of Sciences of The Czech Republic, Cukrovarnicka 10, 16200 Prague, Czech Republic*
[4]*B.I. Stepanov Institute of Physics, National Academy of Sciences of Belarus, Nezalezhnastsi Avenue 68, 220072 Minsk, Belarus*

***Corresponding author**
Dr. Roberto Lorenzi
email address: roberto.lorenzi@unimib.it
phone +39 026448 5169
fax +39 026448 5400

Keywords

Glasses; photoluminescence; radioluminescence; Energy Transfer; Fluorescence

Abstract

Optical properties of yttria-aluminoborate (YAB) glasses with general composition $10(Ce_xTb_yY_{(1-x-y)})$-$30Al_2O_3$-$60B_2O_3$ are investigated and compared with data available on YAB crystals with huntite-like structure. Ce doped samples show optical features ascribable to preferential location of rare earth ions in sites with specific geometry similar to that observed in crystalline structures. Samples prepared with Tb ions as emission activator and Ce ions as sensitizer have been studied within the framework of non-radiative energy transfer. The resulting Förster radius is of 4.6±0.5 Å comparable with that observed in Ce/Tb co-doped $YAl_3(BO_3)_4$ crystals. The investigated materials possess radio- and photoluminescence emission efficiencies and performances comparable to that of crystalline counterparts with the advantage of having easiness of preparation and workability typical of glassy systems.

1. Introduction

Glasses doped with rare earths (RE) are among the materials of choice in advanced optical and scintillator applications. Although their performances are generally less effective than those reported in single- and polycrystals [1], their amorphous structure possesses unique benefits. In particular, their synthesis is a cost-effective preparation strategy readily implementable in large scale production. Glasses present also the advantage of fine chemical tuning dictated only by batch composition. Finally, they are easily workable and can be prepared in a variety of forms and geometry including optical fibres. In particular, yttria-aluminoborate (YAB) and, more generally, lanthanide oxide-aluminoborate glasses have been proved to be a suitable matrix for RE incorporation and for the realization of optical materials thanks to their chemical durability, high transparency and mechanical strength [2-6]. Within the compositions available in the glass-forming region of the Y_2O_3-Al_2O_3-B_2O_3 system [2, 7], a relevant role as possible interesting optical materials can be found for composition with molar ratios close to that of $YAl_3(BO_3)_4$. In YAB crystals this composition leads to the formation of a stable form, isostructural to natural huntite ($Mg_3Ca(CO_3)_4$) crystal [8, 9], which has been extensively studied for the realization of active material for laser technology [10, 11], non-linear optics [12], phosphors [13, 14], and scintillators [15]. In huntite-like YAB crystals Y^{3+}, Al^{3+}, and B^{3+} ions are surrounded by 6, 6, and 3 oxygen atoms in trigonal prism, distorted octahedral, and triangles configuration, respectively. YO_6 trigonal prisms are isolated by BO_3 triangles, while AlO_6 octahedra are arranged in twisted columns by vertex-sharing, each $(AlO_6)_n$ column is linked to the adjacent by BO_3 triangles [16-18], as a result, such systems display large minimum distance between RE atoms [18, 19]. However, these crystals melt incongruently and usually they are prepared by flux methods, preventing a simple and effective preparation route for large single crystals [18, 20]. In the case of YAB and lanthanum oxide-aluminoborate glasses, for suitable compositions, it is possible to obtain amorphous materials where the randomly distributed units have common features with the huntite-like structure. In fact, it has been demonstrated that the amorphous matrix is virtually free from Ln-O-Ln. Thus these glasses have the unusual property of ensuring a minimal distance between Ln ions as high as 6.7 Å [21]. As a result, the possibility of detrimental concentration quenching effects drastically diminishes even at concentration of $30x10^{20}$ Ln atoms/cm^3 making these glasses the ideal hosts for RE-activated optical materials [22].

Here we present a detailed analysis of radio- and photoluminescence properties of YAB glasses with general huntite-like composition –$10Y_2O_3 \cdot 30Al_2O_3 \cdot 60B_2O_3$– and with yttrium ions substituted by Ce and Tb ions. The results show a preferential location of Ce3+ ions in sites with trigonal prismatic symmetry similar to that found in crystalline YAB. Moreover, for the first time, we also investigated the radioluminescence efficiency of these glasses co-doped with Tb and Ce ions evidencing performances comparable to commercial single-crystal materials.

2. Experimental

2.1 Glass preparation

Glasses were prepared using CeO_2 (special purity grade), Tb_3O_4 (special purity grade), Y_2O_3 (special purity grade), $Al(OH)_3$ (analytical grade), H_3BO_3 (chemically pure), Sb_2O_3 (analytical grade) in batches calculated to yield 20 g of glass. Glasses have general formula $10Ln_2O_3 \cdot 30Al_2O_3 \cdot 60B_2O_3$ where Ln is either Y, Ce, or Tb, and Sb_2O_3 powder was added as reducing agent above 100 mol% composition to favour the reduction of CeO_2 to Ce_2O_3. Appropriate proportions of reagents were weighed to an accuracy of 1 mg on an analytical balance so as to obtain samples with molar compositions reported in Tab. 1. The batches were melted in uncovered Pt crucible (about 45 ml) in an electrically heated furnace at 1480 °C for 60 min. The melt was poured onto a stainless steel plate and quenched by being pressed with another stainless steel plate to obtain samples of about 2 mm of thickness. After that the glasses were annealed at 660 °C for 3h and finally allowed to slowly cool down to room temperature. X-ray diffraction patterns confirmed the absence of any spurious crystalline features [21]. Samples were then cut, polished, and prepared as necessary for subsequent measurements.

	Molar composition* (%)					
Label	Tb_2O_3	Ce_2O_3	Y_2O_3	Al_2O_3	B_2O_3	Sb_2O_3
1%Ce	0	1	9	30	60	1
3%Ce	0	3	7	30	60	1
9%Ce	0	9	1	30	60	1
1%Tb:1%Ce	1	1	8	30	60	1
3%Tb:1%Ce	3	1	6	30	60	1
6%Tb:1%Ce	6	1	3	30	60	1
9%Tb:1%Ce	9	1	0	30	60	1
6%Tb	6	0	4	30	60	1

Tab. 1: Label and molar composition of investigated samples. *Sb_2O_3 was added above 100 mol% composition.

2.2 Optical characterization

Photophysical properties of the materials have been investigated by radioluminescence (RL) and time-resolved photoluminescence (PL) techniques. Radioluminescence measurements were carried out at room temperature using two different home-made instruments, both systems have been inter-calibrated by reference samples and all spectra were corrected for spectral responses. In the first apparatus, the detection system comprised a charge coupled device (Jobin Yvon Spectrum One 3000) coupled to a spectrograph operating in the 200-1100 nm range (Jobin Yvon Triax 180). RL excitation was obtained by X-rays irradiation through a Be window, using a Philips 2274 X-ray tube with tungsten target operated at 40 kV and 40 mA. The second apparatus was equipped with a single-grating monochromator and a photon counting detector TBX-04 and excitation was supplied by a molybdenum X-ray tube operating at 40 kV and 15 mA.

PL spectra were collected by means of an Edinburgh FLS980 fluorescence spectrometer with an emission bandpass of 5 nm and operating in Time Correlated Single Photon Counting configuration with pulsed LED source at 250 nm. Photoluminescence excitation (PLE) spectra were measured by a custom-made spectrofluorometer Horiba Jobin Yvon 5000M using a steady state deuterium lamp as light source and using a single-grating monochromator and a photon counting detector TBX-04 as detection system. Decay curves were collected either with the Edinburgh FLS980 apparatus or the Horiba Jobin Yvon 5000M, using an Edinburgh EPLED (emission at 250 nm, pulse width 950 ps) or a Horiba nanoLED (emission at 310 nm, pulse width 200 ps) as excitation sources, respectively. Excitation and emission spectra were corrected for spectral dependence of incident light energy and instrumental responses, respectively. Convolution procedure was applied to the decay curves to determine decay times (SpectraSolve software package, Ames Photonics) in multiexponential fitting.

3. Results and discussion

3.1 Photophysics of Ce doped samples

Photoluminescence emission and excitation spectra of samples doped with 1, 3, and 9 mol% of Ce_2O_3 are shown in Fig. 1a. The main emission band is centred at about 3.51 eV and corresponds to the 5d→4f Laporte-allowed transition of Ce^{3+}. Analysis of Gaussian components of this band evidences the presence of two different contributions with maxima at 3.39 and 3.60 eV, and with a full width at half maximum (FWHM) of 0.68 and 0.54 eV, respectively. Positions, FWHMs, and relative amplitudes of these bands slightly vary with Ce content, the same behaviour can be appreciated up to doping level of 9 mol% and in the radioluminescence spectra reported in Fig. 1b. The observed energy separation of 0.21 eV is consistent with the expected spin-orbit splitting of the $4f^1$ ground state in the $^2F_{5/2}$ and $^2F_{7/2}$ levels. Remarkably, in amorphous hosts the ^2F_j ground state separation is generally hindered by inhomogeneous broadening and usually is not spectrally resolved in the two *j*-components. Indeed, huntite-like glasses seem to maintain a topological crystalline-like order [23]. For our composition, it is expected that the majority of Y atoms (up to 70%) have a bonding state similar to that found in $YAl_3(BO_3)_4$ crystals [24, 25]. For this reason, these glasses manifest the occurrence of peculiar spectroscopic features representative of both crystalline and amorphous states. A clear demonstration of this effect can be found in the PLE spectra reported in Fig. 1a. In this case the composite band can be fitted with three to five Gaussian depending on Ce content. Actually, the $5d^1$ excited state is by far more sensible to crystal field splitting with respect to the $4f^1$ ground level. Thus the $5d^1$ degeneracy is governed by the Ce^{3+} nearest neighbours geometry. Specifically, Ce ions in YAB crystals are expected to occupy a site with D_{3h} (trigonal prismatic) or D_3 (distorted trigonal prismatic with basal triangles slightly twisted one to each other) site symmetry [26]. From group theory and crystal field analysis, the D_{3h} and D_3 symmetries split the *d*-level in 3 and 2 levels, respectively. Indeed, the excitation spectra of samples doped with 1 and 3 mol % of Ce_2O_3 resemble those of Ce^{3+} located in a trigonal prisms as observed in several borate crystals [15, 27-29] rather than in a disordered environment. However, for higher levels of doping the glass network relaxes towards more disordered structure. As a consequence, Ce ions experience a lower symmetry, the 5-fold *d*-level degeneracy is fully removed, and the resulting excitation spectrum became similar to that registered in glassy materials [30-32]. Lastly, the PL intensities scale with Ce content, as reported in Fig. 1c. The recorded amplitudes at peak maximum, normalized for sample 1% Ce, are 0.8 and 0.4 for sample 3% Ce and 9% Ce, respectively. The origin of such behaviour can be explained on the basis of two possible mechanisms: 1) the luminescence intensity is lowered by concentration quenching phenomena

and/or 2) the ratio of Ce^{3+}/Ce^{4+} population is Ce-content dependent and the PL-silent Ce^{4+} species are more abundant for higher Ce concentration, furthermore the presence of Ce^{4+} introduces strong absorption bands at 4.8 eV [33], due to charge-transfer and confirmed by absorption measurements (not shown), that increases the probability of non-radiative energy transfer from Ce^{3+} PL. Nonetheless, the RL intensities increase with Ce content and the maximum amplitudes, normalized to 1% Ce sample, are 1.3 and 1.5 for samples 3% Ce and 9% Ce, respectively. This reflects two different excitation processes for RL and PL, proving a matrix contribution in harvesting energy from ionizing radiation that subsequently is transferred to Ce^{3+} ions. Furthermore, there is the possibility that part of the Ce^{4+} ions even if, in principle, are both PL and RL inactive may undergo to a transient charge change due to electron capture [34] or to other charge-mediated optically active complex [35, 36]. Ce^{4+} ions can thus be temporarily present as Ce^{3+} giving rise to luminescence. This process is indeed peculiar of radio-induced excitation, since near-UV photons have not enough energy to promote electrons from the valence to the conduction band. In this view, the RL is expected to be more efficient than PL and with a less pronounced dependence from Ce^{3+}/Ce^{4+} population. Time-resolved PL analysis gave us some insight about these aspects. The results are summarized in Fig. 2 where the decay curves of Ce-doped samples registered at 365 nm and excited at 310 nm (Fig. 2a) do not show any dramatic effect due to concentration quenching. Being a Laporte-allowed transition, the lifetime of the 5d→4f transition is relatively short and it is of the order of tens of ns. A reliable comparison between kinetic data can be obtained analysing the decay curves as probability density functions, without any assumption on the model at the basis of the physical process, and considering the expected values of the mean lifetime, defined as:

$$\langle \tau \rangle = \frac{\int_{t_0}^{t_f} I(t) t dt}{\int_{t_0}^{t_f} I(t) dt} \qquad \textbf{Eq. 1}$$

where the integral is from t_0 = 0 ns to t_f = 500 ns and $I(t)$ is the PL amplitude as a function of time. The values of $\langle \tau \rangle$ is 25, 21, and 18 ns for samples doped with 1%, 3%, and 9% of Ce_2O_3, respectively. As a matter of fact, the mean lifetime of the highest doped samples is ~80% of the lowest doped one. On the one hand, this result mainly probes concentration quenching effects and cannot give information on possible changes of the relative Ce^{3+}/Ce^{4+} population. On the other hand, some indication can be derived from the PL

spectra reported in Fig. 1. These spectra have been taken with comparable instrumental and sample geometry conditions and, as a consequence, their relative amplitude can be assumed proportional to the luminescence quantum yield. If this regime is valid then the reported intensities are sensitive both to the lowering of the radiative lifetime arising from concentration quenching and to the population of excited Ce^{3+} ions. However, the discrepancy observed in the total luminescence efficiency between 1% and 9% Ce samples (see Fig. 1) is about half than the expected 80% coming from decay curve analysis. This is probably related to different Ce/Sb relative concentrations that modify the Ce^{3+}/Ce^{4+} ratio. In fact, Sb is a well-known reducing agent for glasses [37, 38] and a higher concentration of Ce^{3+} is expected in samples with a higher number of Sb ions per atom of Ce. Accordingly, keeping fixed the Sb concentration, the PL intensity inversely scales with Ce content. Decay curves in Fig. 2a can be analysed in more detail as sum of two exponentials. This feature is quite common in glassy materials, and it is usually connected to the presence of different preferential locations of Ce ion in the network [39]. To further investigate this aspect, we have collected time-resolved photoluminescence emission spectra (TRPLE). The contour plot of TRPLE (Fig. 2b) shows a peak maximum shifting from 3.6 to 3.4 eV as the time passes from 0 to 100 ns. The sliced time-resolved TRPLE reported in Fig. 2c evidences this situation. In particular, the spectrum collected after 5 ns is not only shifted to higher energies, but it also features a smaller FHWM with respect to the spectrum collected after 100 ns. These two different recombinations can be ascribed to cerium ions located in two different positions, even if with similar local symmetry as expected also in YAB single crystals doped with yttrium-substituting rare earths [40].

3.2 Photophysics of Ce/Tb codoped samples

Starting from the considerations of the previous section, we prepared a series of Ce/Tb codoped glasses with huntite-like composition with the intent of enhancing luminescence properties through energy transfer from Ce ions to Tb ions. The results of RL experiments on samples doped with 1% Ce_2O_3 and 1%, 3%, 6%, and 9% of Tb_2O_3 are reported in Fig. 3a. Spectra show the typical emission bands of Tb^{3+} ions, characterized by a multiplet in the green region with sharp peaks at 2.0, 2.1, 2.2, 2.3 and 2.5 eV and corresponding to the $^5D_4 \rightarrow {}^7F_j$ transitions. As summarized in Fig. 3b, the addition of Tb ions causes two main effects on the registered PL amplitude: 1) an increase of the Tb-related emissions in the 2.0-2.5 eV and 2) a decrease of the

Ce-related emission in the 2.8-3.8 eV region. These experimental evidences can be attributed to energy transfer processes between Ce and Tb ions acting as donor and acceptor species, respectively. This process enhances the overall emission efficiency of the system, leading to a glass-based material with RL performances comparable to commercial single crystal scintillating materials. In fact, the amplitude at peak maximum for the sample 9%Tb:1%Ce is about 5 times higher than that registered for the single-crystal of $Bi_4Ge_3O_{12}$ (BGO), used as standard in scintillation, while the integrated intensity is 85% with respect to BGO. Moreover, the introduction of 1% Ce indeed enhances the Tb emission and the RL intensity of sample 6%Tb:0%Ce (red cross in Fig. 3b) is about half of that for 6%Tb:1%Ce. Similar results have been obtained in PL experiments, as reported in Fig. 4a. Once more, the integrated emission of Tb scales with its content and, conversely, the Ce signal decreases. To quantify the energy transfer process, we monitored Ce^{3+} decay (i.e. the donor species) at 365 nm, and excited at 250 nm, as a function of Tb content (i.e. the acceptor species). As expected, increasing the acceptor concentration accelerates the donor decay (see Fig. 4b), passing from a mean lifetime of 25 to 8 ns for Tb-free and 9%Tb:1%Ce sample, respectively. Starting from the mean lifetime $\langle\tau_0\rangle = 25$ ns of the donor species in absence of any acceptor and the lifetime $\langle\tau\rangle$ in presence of the acceptor, we have calculated the energy transfer efficiency $\Phi_{ET} = 1 - \langle\tau\rangle/\langle\tau_0\rangle$ as a function of Tb concentration. The result is summarized in Fig. 4c, where it is shown that Φ_{ET} monotonically increases with Tb content up to 68% registered for the sample with the highest content of Tb ions. Data in Fig. 4c have been fitted within the theoretical framework of Förster energy transfer to evaluate the critical concentration C_0 at which there is, on average, one acceptor atom in a sphere of radius R_0 centred on the donor atom [41, 42]. Where the latter radius is the so-called Förster radius defined as the critical distance between donors and acceptors at which the energy transfer efficiency is 50%. C_0 was obtained by fitting data in Fig. 4c with the following formula:

$$\Phi_{ET} = \sqrt{\pi} x \exp x^2 \, (1 - \mathrm{Erf}\, x)$$
$$x = \frac{\sqrt{\pi}}{2}\frac{C}{C_0} \qquad \textbf{Eq. 2}$$

where C is the acceptor concentration expressed in the same units of C_0 and Erf is the error function. Finally, if C_0 is expressed in atoms/cm^3 then the Förster radius can be calculated as:

$$R_0(\mathrm{cm}) = \sqrt[3]{\frac{3}{4\pi C_0(\mathrm{atoms/cm^3})}} \qquad \textbf{Eq. 3}$$

In addition, for a consistent comparison with crystals with similar composition, in Fig. 4c we show in red lines the fitting results using Eq. 2 carried on our data and on literature data on Ce/Tb codoped $YAl_3(BO_3)_4$ crystals with huntite structure (empty squares in Fig. 4c) collected by Blasse et al. [43]. The fitted values of C_0 are 2.5x10^{21} atoms/cm^3 and 1.5x10^{21} atoms/cm^3 for our glasses and YAB crystals, respectively, after correction for the density of glass [44] (3.15 g/cm^3) and crystal[45] (3.73 g/cm^3) and the slight different definition of molar composition used by us and by Blasse. These values correspond to Förster radii of 4.6±0.5 Å and 5.4±0.5 Å for our glasses and huntite crystals, respectively. Interestingly, the two radii are of comparable extension. This outcome is a further confirmation that glass structure recalls that of the parent crystals without altering the overall optical properties.

Conclusion

The optical characterization of YAB glasses presented in this work shows that these systems are a suitable family of amorphous solids for the incorporation of rare-earth. From time resolved PL analysis we have demonstrated that Ce emission is not compromised even at doping levels as high as 9 % mol. For low doping level, Ce ions are preferentially located in positions with trigonal prismatic geometry as occurs in huntite-like single crystals with similar composition. In addition, Ce ions can be appropriately used as activator species to intensify Tb^{3+} luminescence resulting in a glassy system with RL efficiency comparable to BGO crystals. Finally, Förster radii calculated for our YAB glass are comparable with those calculated for Ce/Tb doped YAB crystals. The results obtained in this work reveal that this family of glasses represents a promising candidate as scintillating and photonic material.

Conflicts of interest

There are no conflicts to declare.

Acknowledgements

RL acknowledges the financial support by Cariplo Foundation, Italy, under projects 2012-0920 and 2014-1971. The authors acknowledge the financial support of H2020-TWINN-2015 "*ASCIMAT*", no. 690599 (2016-2019), Ministry of Education and Science of the Russian Federation under Grant 14.Z50.31.0009, and Belarusian Republican Foundation for Fundamental Research, project no. F16R-025. The authors would like to thank Dr. E. Kh. Mamadzhanova and Dr. E.S. Ignat'eva for assistance in preparation of some samples and Prof. A. Vedda for useful discussions.

References

[1] M.J. Weber, J. Lumin., 100 (2002), pp. 35-45.
[2] H.L. Rutz, D.E. Day, C.F. Spencer, J. Am. Ceram. Soc., 73 (1990), pp. 1788-1790.
[3] D. Lemesh, J. Shelby, Phys. Chem. Glasses, 45 (2004), pp. 1-6.
[4] C. Santos, D. Mohr, W. Silva, A.S.S. de Camargo, H. Eckert, M. Li, M. Vermelho, A.C. Hernandes, A. Ibanez, C. Jacinto, J. Appl. Phys., 106 (2009), p. 023512.
[5] V.F. Guimarães, L.J. Maia, I. Gautier-Luneau, C. Bouchard, A.C. Hernandes, F. Thomas, A. Ferrier, B. Viana, A. Ibanez, J. Mat. Chem. C, 3 (2015), pp. 5795-5802.
[6] G. Gao, J. Wei, Y. Shen, M. Peng, L. Wondraczek, J. Mat. Chem. C, 2 (2014), pp. 8678-8682.
[7] I.N. Chakraborty, H. Rutz, D.E. Day, J. Non-Cryst. Solids, 84 (1986), pp. 86-92.
[8] D. Graf, W. Bradley, Acta Crystallographica, 15 (1962), pp. 238-242.
[9] W. Doness, R. Rpsoen, Am. Mineral., 71 (1986), pp. 163-166.
[10] P. Wang, J.M. Dawes, P. Dekker, J.A. Piper, Optics communications, 174 (2000), pp. 467-470.
[11] E. Volkova, V. Markin, N. Leonyuk, J. Cryst. Growth, (2016).
[12] S. Ilas, P. Loiseau, G. Aka, T. Taira, Opt. Express, 22 (2014), pp. 30325-30332.
[13] R.S. Kumar, V. Ponnusamy, V. Sivakumar, M. Jose, Journal of Rare Earths, 32 (2014), pp. 927-932.
[14] P. Liu, J. Liu, X. Zheng, H. Luo, X. Li, Z. Yao, X. Yu, X. Shi, B. Hou, Y. Xia, J. Mat. Chem. C, 2 (2014), pp. 5769-5777.
[15] O. Aloui-Lebbou, C. Goutaudier, S. Kubota, C. Dujardin, M.T. Cohen-Adad, C. Pedrini, P. Florian, D. Massiot, Opt. Mater., 16 (2001), pp. 77-86.
[16] N. Ye, J.L. Stone-Sundberg, M.A. Hruschka, G. Aka, W. Kong, D.A. Keszler, Chem. Mater., 17 (2005), pp. 2687-2692.
[17] P. Plachinda, E. Belokoneva, Cryst. Res. Technol., 43 (2008), pp. 157-165.
[18] N. Leonyuk, L. Leonyuk, Prog. Cryst. Growth Charact. Mater., 31 (1995), pp. 179-278.
[19] F. Auzel, P. Goldner, Opt. Mater., 16 (2001), pp. 93-103.
[20] J. Li, J. Wang, X. Cheng, X. Hu, X. Wang, S. Zhao, Mater. Lett., 58 (2004), pp. 1096-1099.
[21] G. Malashkevich, V. Sigaev, N. Golubev, E.K. Mamadzhanova, A. Sukhodola, A. Paleari, P. Sarkisov, A. Shimko, Mater. Chem. Phys., 137 (2012), pp. 48-54.
[22] G. Malashkevich, N. Golubev, E.K. Mamadzhanova, M. Ziyatdinova, V. Sigaev, A. Sukhodola, T. Khotchenkova, I. Prusova, I. Sergeev, Glass Ceram., 70 (2013), pp. 141-142.
[23] A.C. Wright, J. Non-Cryst. Solids, 401 (2014), pp. 4-26.
[24] H. Deters, A.S. de Camargo, C.N. Santos, C.R. Ferrari, A.C. Hernandes, A. Ibanez, M.T. Rinke, H. Eckert, J. Phys. Chem. C, 113 (2009), pp. 16216-16225.
[25] H. Deters, A.S. de Camargo, C.N. Santos, H. Eckert, J. Phys. Chem. C, 114 (2010), pp. 14618-14626.

[26] A. Watterich, P. Aleshkevych, M. Borowiec, T. Zayarnyuk, H. Szymczak, E. Beregi, L. Kovacs, J. Phys.: Condens. Matter, 15 (2003), p. 3323.
[27] F. Kellendonk, T. Van den Belt, G. Blasse, J. Chem. Phys., 76 (1982), pp. 1194-1201.
[28] Q. Zhang, H. Ni, L. Wang, F. Xiao, Ceram. Int., 42 (2016), pp. 6115-6120.
[29] G. Blasse, A. Bril, J. Chem. Phys., 47 (1967), pp. 5139-5145.
[30] N. El Jouhari, C. Parent, G. Le Flem, J. Solid State Chem., 123 (1996), pp. 398-407.
[31] H. Ebendorff-Heidepriem, D. Ehrt, Opt. Mater., 15 (2000), pp. 7-25.
[32] G. DasMohapatra, Mater. Lett., 35 (1998), pp. 120-125.
[33] A. Vedda, N. Chiodini, D. Di Martino, M. Fasoli, F. Morazzoni, F. Moretti, R. Scotti, G. Spinolo, A. Baraldi, R. Capelletti, Chem. Mater., 18 (2006), pp. 6178-6185.
[34] F. Moretti, A. Vedda, N. Chiodini, M. Fasoli, A. Lauria, V. Jary, R. Kucerkova, E. Mihokova, A. Nale, M. Nikl, J. Lumin., 132 (2012), pp. 461-466.
[35] V. Arbuzov, M. Tolstoi, M. Elerts, Y.S. Trokshs, Sov. J. Glass Phys. Chem.;(United States), 13 (1988).
[36] V. Arbuzov, V. Grabovskis, Y. Dzenis, Glass Phys. Chem, 18 (1992), p. 147.
[37] J.M. Parker, Coloration Technology, 34 (2004), pp. 26-38.
[38] M. Hujova, M. Vernerova, Ceramics–Silikáty, 61 (2017), pp. 119-126.
[39] M. Fasoli, A. Vedda, A. Lauria, F. Moretti, E. Rizzelli, N. Chiodini, F. Meinardi, M. Nikl, J. Non-Cryst. Solids, 355 (2009), pp. 1140-1144.
[40] M. Ramirez, L. Bausá, D. Jaque, E. Cavalli, A. Speghini, M. Bettinelli, J. Phys.: Condens. Matter, 15 (2003), p. 7789.
[41] T. Főrster, Discussions of the Faraday Society, 27 (1959), pp. 7-17.
[42] M. Inokuti, F. Hirayama, J. Chem. Phys., 43 (1965), pp. 1978-1989.
[43] G. Blasse, A. Bril, J. Chem. Phys., 47 (1967), pp. 1920-1926.
[44] M. Ziyatdinova, N. Golubev, E. Ignat'eva, A. Okhrimchuk, T. Khotchenkova, V. Sigaev, Glass Ceram., 72 (2016), pp. 366-369.
[45] YAl3B4O12 (YAl3[BO3]4) Crystal Structure: Datasheet from "PAULING FILE Multinaries Edition – 2012" in SpringerMaterials, in: P. Villars, K. Cenzual (Eds.), Springer-Verlag Berlin Heidelberg & Material Phases Data System (MPDS), Switzerland & National Institute for Materials Science (NIMS), Japan.

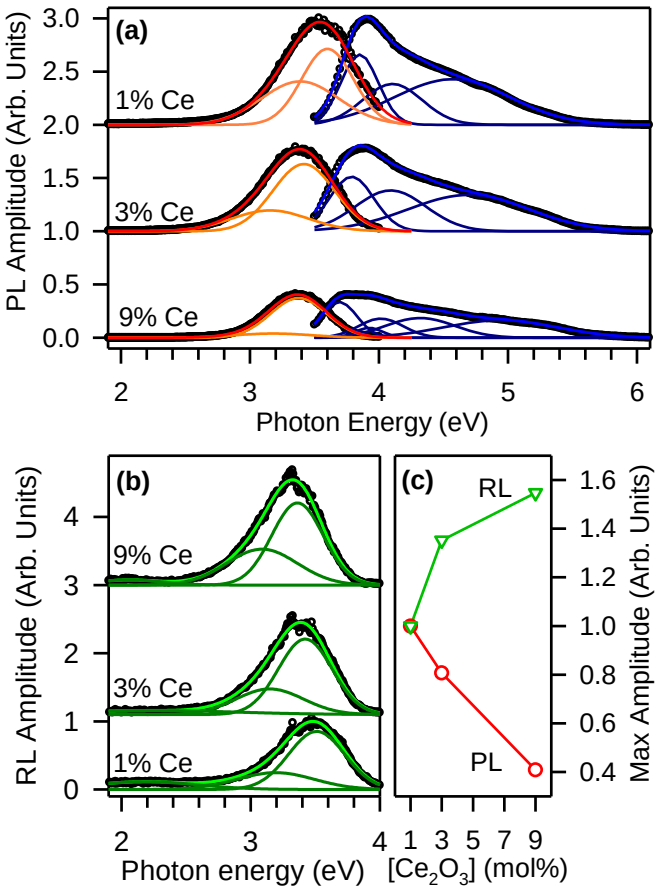

Fig. 1. Photoluminescence emission excited at excitation peak maximum (red colours, (a)), excitation of the maximum emission peak (blue colours, (a)), and radioluminescence (green colours, (b)) spectra of Ce doped glasses with huntite-like composition. Spectra were reconstructed by using the minimum number of necessary Gaussian bands. Spectra are normalized with respect to 1% Ce sample and are upshifted for clarity. (c) Maximum PL (red circles) and RL amplitudes (green triangles) as a function of Ce_2O_3 molar content.

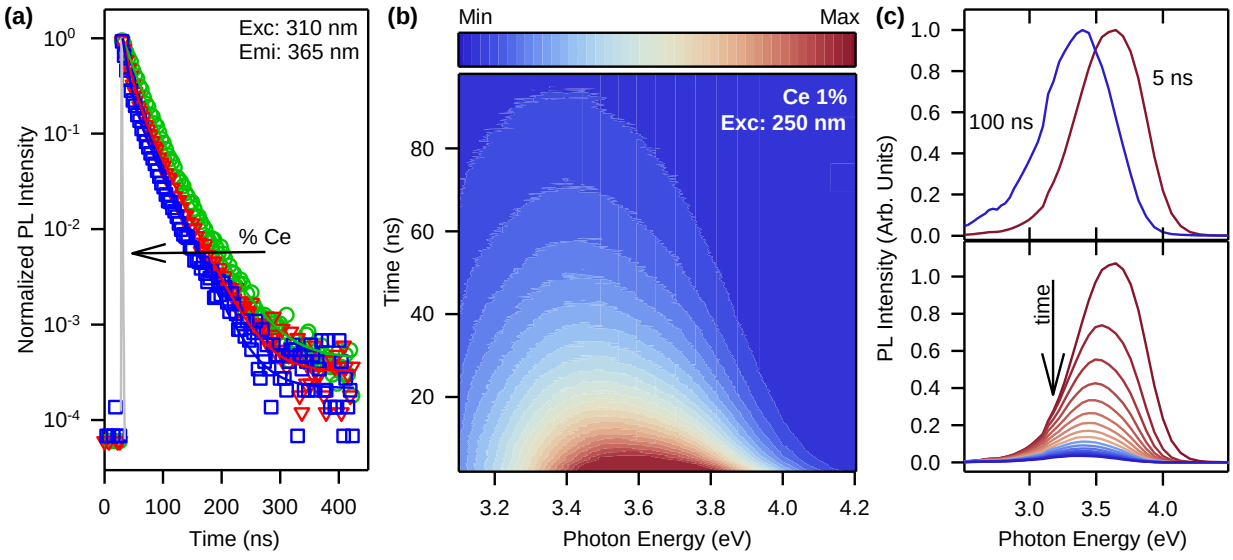

Fig. 2. (a) Decay curves for samples containing 1% (green circles), 3% (red triangles), and 9% (blue squares) of Ce_2O_3, grey solid line is the signal of the laser pulse, solid lines represent fitting with a sum of two

exponentials. Spectra were collected with excitation and emission wavelengths of 310 and 365 nm, respectively. (b) Contour plot of time-resolved photoluminescence emission (TRPLE) spectra collected on sample with 1 % Ce, a nanosecond LED operating at 250 nm was used as excitation source. (c) In the lower panel, sliced TRPLE of (a) from 5 to 100 ns in steps of 5 ns and, in the upper panel, normalized emission spectra at 5 (red curve) and 100 ns (blue curve).

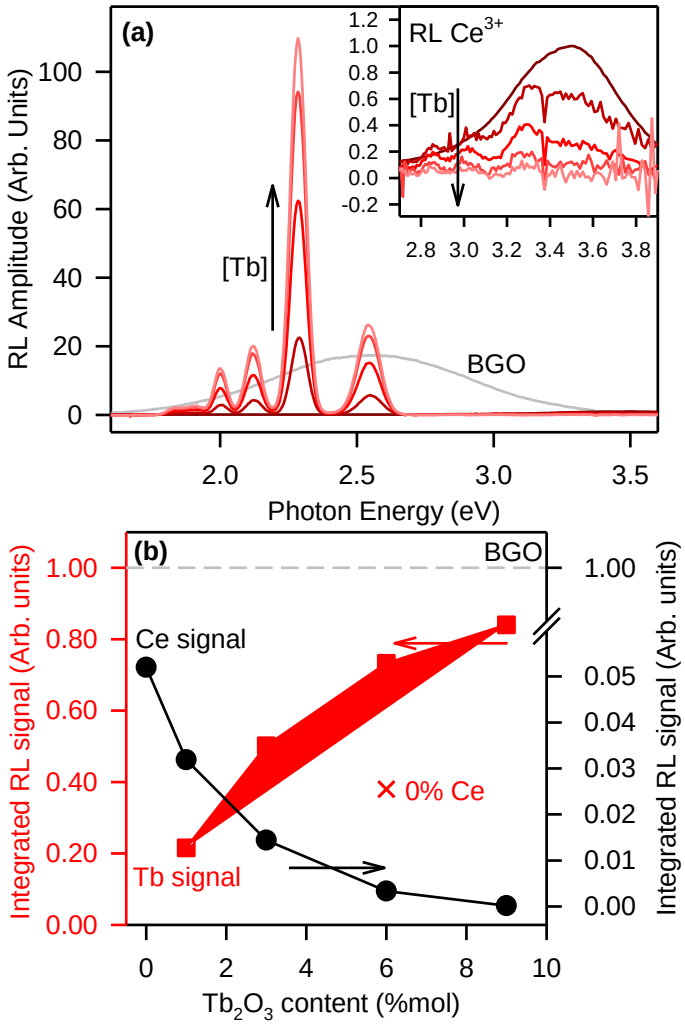

Fig. 3. (a) Radioluminescence of samples doped with 1 mol % of Ce_2O_3 and 0, 1, 3, 6, and 9 mol % of Tb_2O_3 (red coloured lines) and reference signal of $Bi_4Ge_3O_{12}$ single crystal (grey line). In the inset: amplified scale in the region of Ce emission. All spectra are normalized for the maximum amplitude registered for sample 1 % Ce. (b) Integrated RL signal in the Tb emission region from 1.9 to 2.6 eV (red squares, left axis) and in the Ce emission region from 2.8 to 3.9 eV (black circles, right axis). The red cross mark indicates the integrated RL signal of Tb emission in the sample doped with 6 mol % of Tb_2O_3 and without Ce doping. All integrated values are normalized to the integrated signal of $Bi_4Ge_3O_{12}$.

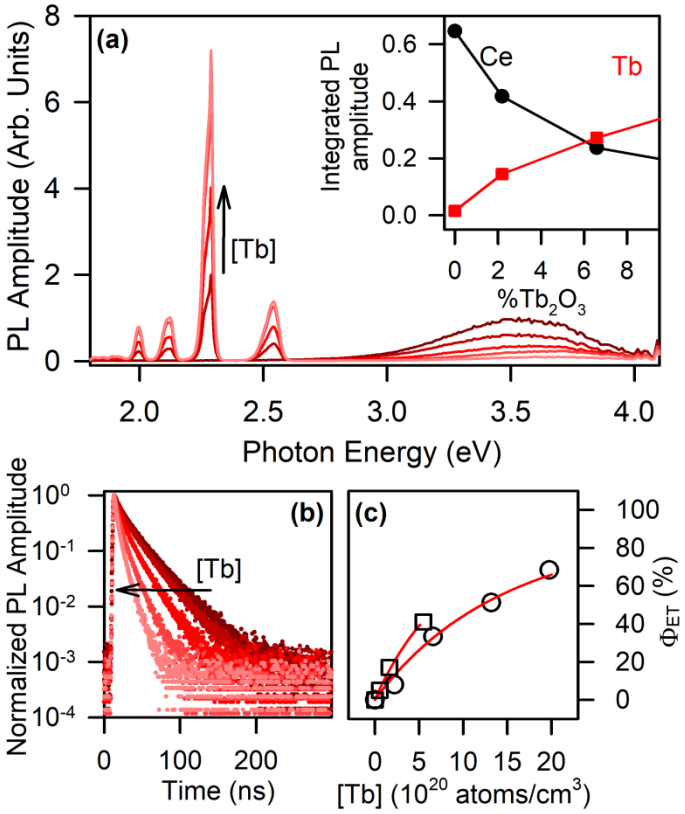

Fig. 4. (a) Photoluminescence of samples doped with 1 mol % of Ce_2O_3 and 0, 1, 3, 6, and 9 mol % of Tb_2O_3. All spectra are normalized for the maximum amplitude registered for sample 1 % Ce. In the inset: integrated PL signal in the Tb emission region from 1.9 to 2.6 eV (red squares) and in the Ce emission region from 2.8 to 3.9 eV (black circles). (b) Time resolved Ce emission of samples reported in (a), spectra were collected with excitation and emission wavelengths of 250 and 365 nm, respectively. (c) Energy transfer efficiency as a function of Tb doping for glasses studied in this work (empty circles) and from Ce/Tb codoped $YAl_3(BO_3)_4$ single crystals from Ref. [43] (empty squares). Red lines represent fitting result using Eq. 2 with C_0 as the only free parameter.